Quantifying the validity conditions of the Beckmann-Kirchhoff scattering model

Helia Hooshmand*, Mingyu Liu, Richard Leach, Samanta Piano
Manufacturing Metrology Team, Faculty of Engineering, University of Nottingham, Nottingham, UK

ABSTRACT

Approximate and rigorous methods are widely used to model light scattering from a surface. The boundary element method (BEM) is a rigorous model that accounts for polarisation and multiple scattering effects. BEM is suitable to model the scattered light from surfaces with complex geometries containing overhangs and re-entrant features. The Beckmann-Kirchhoff (BK) scattering model, which is an approximate model, can be used to predict the scattering behaviour of slowly-varying surfaces. Although the approximate BK model cannot be applied to complex surface geometries that give rise to multiple scattering effects, it has been used to model the scattered field due to its fast and simple implementation. While many of the approximate models are restricted to surface features with relatively small height variations (typically less than half the wavelength of the incident light), the BK model can predict light scattering from surfaces with large height variations, as long as the surfaces are "locally flat" with small curvatures. Thus far, attempts have been made to determine the validity conditions for the BK model. The primary validity condition is that the radius of curvature of any surface irregularity should be significantly greater than the wavelength of the light. However, to have the most accurate results for the BK model, quantifying the validity conditions is critical. This work aims to quantify the validity conditions of the BK model according to different surface specifications, e.g., slope angles and curvatures. For this purpose, the scattered fields from various sinusoidal profiles are simulated using the BEM and the BK models and their differences are compared. The result shows that the BK model fails when there are high slope angles and large curvatures, and these conditions are quantified.

Keywords: light scattering, boundary element method, Beckmann-Kirchhoff, validity conditions, slope and curvature

*Helia.Hooshmand@nottingham.ac.uk; https://www.nottingham.ac.uk/research/manufacturing-metrology

1. INTRODUCTION

When a light beam illuminates an object with surface height variations of the order of or larger than the incident wavelength, the object scatters the light in various directions[1, 2], while in an optically flat object, specular reflection is dominant. For a certain object material and illumination condition (fixed incident angle, wavelength and polarisation), the scattering pattern depends on the surface topography of the object, and can be used to reveal topography information [2]. In conventional three-dimensional (3D) optical surface topography measurement instruments, e.g. coherence scanning interferometry (CSI), confocal microscopy and focus variation microscopy, the scattered field propagates through the optical instrument to form the raw images. The 3D surface topography is then obtained using an appropriate surface reconstruction method, e.g. envelope detection[3], frequency domain analysis[4] and the correlogram correlation method[5] in interference microscopy, contrast measurement methods in focus variation microscopy[6] and the use of fitting algorithms on the axial response in confocal microscopy[7]. As a result, modelling of light scattering is critical for any optical surface measurement system.

Scattering models can be categorised into two major groups: rigorous and approximate models. In rigorous models, such as the finite difference time domain (FDTD) method[8], finite element method (FEM)[9], rigorous coupled-wave analysis (RCWA)[10] and boundary element method (BEM)[11], numerical techniques are used to solve Maxwell's equations. Rigorous models are complex and can be computationally intensive. However, to predict the scattered light from complex surface geometries containing overhangs and re-entrant features, or other types of geometries where multiple scattering occurs, only rigorous scattering models can be applied. Thus far, various rigorous models have been adopted for confocal[12] and interference microscopy[13-15]. The BEM model solves linear partial differential equations only along the surface boundaries and, therefore, is computationally more efficient to model surface scattering compared to other rigorous models. BEM has

been used in several applications including rigorous speckle simulation[16], modelling of the total electric field induced by transcranial magnetic simulation[17], development of acoustic holography algorithms for spatial transformation of sound fields radiated by irregularly shaped sources[18], development of a stable time domain method for the analysis of electromagnetic scattering and radiation problems[19], signal modelling in CSI for a vee-groove surface type[20] and a range of tilted blazed diffraction gratings[21], and in on-machine surface defect detection using light scattering and deep learning for sawtooth gratings[22].

Approximate scattering models make use of certain approximations to solve Maxwell's equations. Approximation models lead to different limitations in their ranges of validity which make them applicable only on weakly scattering media, surfaces with small height variations and/or slowly varying surfaces on the optical scale. Nevertheless, compared to rigorous methods, approximate models are straightforward to implement and computationally efficient. Furthermore, they provide direct insight into the scattering process and can often deliver an inverse solution to surface determination from the scattering data as they consider light scattering as a linear process[23]. One common approximate model is based on the small height approximation which can only be used on near planar surfaces[24]. The small height approximation relies on the assumption that the phase of the field at each point on the surface is directly proportional to the surface heights so that the surface can be replaced by a thin phase grating. The validity condition of the small height approximation is expressed by the Rayleigh criterion, i.e. $h < \lambda/8$ for normal incident illumination, where h is the surface height variation and λ is the illumination wavelength[2]. The small height approximation along with a 2D representation of the propagating light field (referred to as the elementary Fourier optics model) has been used to model an interference microscope[25]. The Rayleigh-Rice (also known as vector perturbation theory) can relate the surface power spectral density (PSD) of a slightly rough surface to the corresponding scattering pattern[26]. The perturbation approach is valid when the root-mean-square (RMS) of the surface height is small compared to the wavelength of the incident light. A widely used approximate model for weakly scattering medium is the first-order Born approximation[24] in which the total field (incident and scattered fields) can be replaced by the incident field. The main validity condition of the Born approximation is that the refractive index of the scattering medium should only differ slightly from unity.

Among the approximate models, the Beckmann-Kirchhoff (BK) solution (also known as the Kirchhoff approximation) is commonly applied to reduce the theoretical complexity of a rough surface scattering problem[2, 24]. The BK model is not restricted to small height surface variations and can predict light scattering from rough surfaces (i.e. surfaces with larger RMS heights than those used with perturbation methods). The BK model assumes that the local curvatures of the surface are small compared to the wavelength of the incident light, i.e., to fulfil the Kirchhoff approximation, the surface has to be locally flat. Therefore, the Kirchhoff approximation is appropriate for smooth surfaces without sharp edges.

The BK model has been used in various surface topography measurement applications including signal modelling[27, 28] and measurement and correction of the 3D transfer function with CSI[29], 3D image formation in focus variation microscopy[30], modelling the scattered light from rough surfaces[31, 32] and characterisation of laser powder bed fusion surfaces[33]. The validity of the BK model for surface scattering has been investigated in terms of the surface correlation length, angle of the incidence, RMS of heights, and the ratio of the width of the rectangular corrugations and the separation between adjacent corrugations to the incident wavelength[2, 34-36]. However, currently there are no well-established quantitative conditions under which the BK is valid (to the authors' knowledge).

In this paper, the scattered field from a range of sinusoidal with different radii of curvature (ROC) and slope angles - using a range of different pitch and height values - has been simulated using the 2D BK model and the 2D BEM model. The angular distribution of the scattering patterns of each profile obtained by the BK model is compared to those from the BEM model using the RMS of the difference of normalised scattered fields (NSFs). Variation of the RMS of the difference of the NSFs has been investigated in terms of the change in the minimum ROC and maximum slope angle of the profiles. It is shown that the presence of the low ROC (compared to the wavelength of the incident light) and high slope angle (SA) within a profile results in multiple scattering and causes the BK model to fail.

2. RIGOROUS AND APPROXIMATE SCATTERING MODELS

1.1 2.1 Modelling of the scattered field using the rigorous BEM model

The rigorous BEM model used in this work is based on the work by Simonsen[37], while the theory was developed earlier by Maradudin et al.[38]. The BEM model finds the total field and its normal derivative along the surface by taking advantage of the Ewald-Oseen extinction theorem[39] and solves the subsequent set of inhomogeneous integral equations through conversion to matrix equations by appropriate spatial discretisation of the integrals. This approach provides an exact

solution and accounts for the multiple scattering and polarisation effects; therefore, this model is promising for arbitrarily complex surfaces. The 2D version of the BEM algorithm is restricted to prismatic surfaces that can be fully described in the plane of incidence, assuming the surface is infinitely extended along the third dimension, perpendicular to the incidence plane. The scattering outside the incidence plane is considered negligible for prismatic surfaces, and this feature means that the 2D BEM model is able to simulate the scattered field without significant loss of accuracy.

According to the integral theorem of Helmholtz and Kirchhoff[24], the scattered field $E_s(r)$ from any surface can be expressed from the values of the total field $E(r')$ and its normal derivative, $\partial E(r')/\partial n'$ on the surface s

$$E_s(r) = \iint_s \left[G(r-r')\frac{\partial E(r')}{\partial n'} - E(r')\frac{\partial G(r-r')}{\partial n'} \right] ds, \tag{1}$$

where $G(r-r')$ is the Green's function of the Helmholtz operator and $\partial/\partial n'$ denotes differentiation along the outward normal to the surface. In the BEM model, the total field and its normal derivatives at given points on the surface are calculated globally, taking into account the contribution of all neighbouring points. As a result, the BEM model is able to address multiple scattering effects. Accordingly, the scattering surface is divided into several discrete points, and for each point, the Kirchhoff surface integral and the boundary conditions are applied. Values for the field and its normal derivative at each point can be obtained by solving the coupled matrix equations[37]. Eventually, the BEM finds the surface "source" fields, from which the far-field scattering at any point can be calculated.

As an example, the BEM model was applied to a 2D sinusoidal profile with a 15 μm pitch, 1 μm peak-to-valley distance (height) and 225 μm length (includes fifteen cycles). The angular distribution of the NSF and its 2D visualisation in the incidence plane obtained by the 2D BEM are shown in Figure 1 (a) and (b), respectively. The incident illumination was chosen to be a transverse electric field (TE polarisation) with a monochromatic plane-wave ($\lambda = 0.58$ μm) normal to the surface profile. The far-field scattered field was calculated over 777 observation angles sampled from -88° to 88° to cover the widest possible range of the angular distribution.

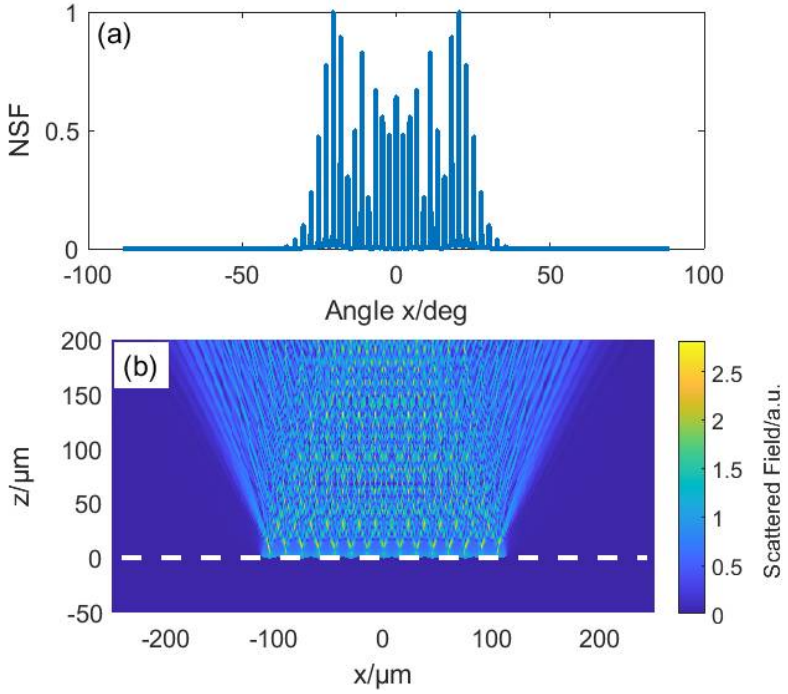

Figure 1. 2D BEM scattered field from a sinusoidal profile with 15 μm pitch, 1 μm height and 225 μm length (a) angular distribution of the NSF (unitless), (b) 2D BEM scattered field in the incidence plane.

1.2 2.2 Modelling of the scattered field using the approximate BK model

Consider a monochromatic plane-wave $E_i(\mathbf{r}) = \exp(2\pi i \mathbf{k_i}.\mathbf{r})$ propagating with the wave vector $\mathbf{k_i}$ illuminating a scattering object. The Kirchhoff boundary conditions approximate the total field (E) and its normal derivative at a surface point $\mathbf{r_s}$ and can be written as[2]

$$E(\mathbf{r_s}) = (1+R)E_i(\mathbf{r_s}), \tag{2}$$

$$\frac{\partial E(\mathbf{r_s})}{\partial n} = 2\pi \mathbf{k_i}.\hat{\mathbf{n}}(1-R)E_i(\mathbf{r_s}), \tag{3}$$

where $\hat{\mathbf{n}}$ is the normal to the surface at $\mathbf{r_s}$, and R is the Fresnel amplitude reflection coefficient (assumed to be constant over the range of desired scattering angles).

Substituting Eqs. (2) and (3), and the free-space Green's function $G = \exp(2\pi i k_0 |\mathbf{r}|)/4\pi|\mathbf{r}|$ into the Kirchhoff surface integral of Eq. (1), the far-field scattered field can be written as[27]

$$\tilde{E}_s(\mathbf{K}+\mathbf{k_i}) = -\frac{1}{2k_0}\delta\left(|\mathbf{K}+\mathbf{k_i}|-k_0\right)\left[\frac{|\mathbf{K}|^2}{\mathbf{K}.\mathbf{z}}\right]\iiint R\delta\left[r_z - Z_s(r_x,r_y)\right]\exp(-2\pi i \mathbf{K}.\mathbf{r})d^3r, \tag{4}$$

where $\mathbf{K} = \mathbf{k_s} - \mathbf{k_i}$ and $\mathbf{k_s}$ is the scattering wave vector (for elastic scattering $|\mathbf{k_s}| = |\mathbf{k_i}| = k_0 = 1/\lambda$). In Eq. (4), the term $R\delta\left[r_z - Z_s(r_x,r_y)\right]$ is referred to as the "foil model" of the surface[27]. Based on the foil model, the object can be replaced by a 1D Dirac delta function representing the value of the reflection coefficient at each point on the surface.

The scattered field over the whole surface is described by a 3D surface transfer function (STF) given by

$$\tilde{G}(\mathbf{K}+\mathbf{k_i}) = \frac{i}{4\pi k_0}\delta\left(|\mathbf{K}+\mathbf{k_i}|-k_0\right). \tag{5}$$

In other words, all possible scattered wave vectors $\mathbf{k_s}$ due to the incident wave vector $\mathbf{k_i}$ construct a spherical shell k_0 (Ewald sphere) in the **K** space, which is centred at $-\mathbf{k_i}$ and has a radius k_0 [40]. Using the definition of the STF, Eq. (4) can be re-written as

$$\tilde{E}_s(\mathbf{K}+\mathbf{k_i}) = 4\pi i\left[\frac{|\mathbf{K}|^2}{\mathbf{K}.\mathbf{z}}\right]\tilde{G}(\mathbf{K}+\mathbf{k_i})\tilde{F}_K(\mathbf{K}), \tag{6}$$

where $\tilde{F}_K(\mathbf{K}) = \iiint R\delta\left[r_z - Z_s(r_x,r_y)\right]\exp(-2\pi i \mathbf{K}.\mathbf{r})d^3r$ is the Fourier transform of the foil model of the object. Eq. (6) shows that in the BK model, the scattering is considered as a linear filter (defined by the STF) applied to the foil model of the surface.

Figure 2 (a) illustrates the 2D foil model of a sinusoidal profile with 15 μm pitch and 1 μm height. In Figure 2(b), the 2D STF with a monochromatic plane wave (λ = 0.58 μm) that is normal to the surface profile is shown. The scattered far-field was calculated over 777 observation angles sampled from -88° to 88°. The angular distribution of the NSF obtained by the 2D BK model is shown in Figure 2 (c).

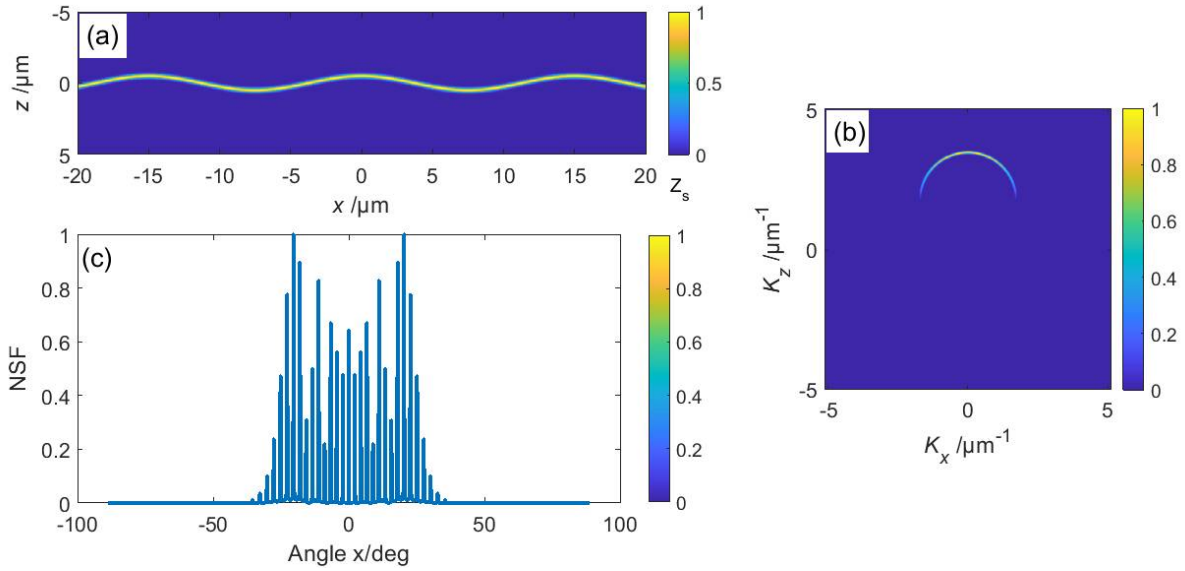

Figure 2. 2D BK scattered field from a sinusoidal profile with 15 µm pitch, 1 µm height and 225 µm length (a) 2D foil model of the surface (generated over the same length, with the display window being trimmed for better visualisation), (b) 2D STF and (c) angular distribution of the NSF (unitless).

3. METHOD

In order to find the validity condition of the approximate BK model, experiments involving quantitative comparisons between the scattered fields obtained by the BK and the BEM models were designed. A range of sinusoidal profiles with various minimum ROCs and maximum SAs were investigated. In each case, the RMS of the differences between the NSF obtained by the BK and the BEM models was calculated. Both models compute the scattered far-fields over the same angular distribution. The range of angles is determined by the sampling resolution of the profile. To obtain accurate far-field scattering results, the surface is sampled equidistantly, with the sampling distance set to be smaller than λ/5. The range of the angular distribution is fixed between -88° to 88°. As the profile is considered to be continuously repeated in the BK model, in order to reasonably compare scattered fields from a sinusoidal profile for the BK and the BEM models, the length of the profile is set to include at least ten cycles. The scattered field from the BEM model is determined by averaging the magnitude of the obtained scattered fields from both TE and TM polarisations of the incident illumination.

4. RESULTS AND DISCUSSION

1.3 4.1 Comparison of the BEM and the BK models for a range of sinusoidal profiles with lengths of ten times the pitch values

Variations of the RMS of the difference of the normalised scattered far-fields obtained by the BEM and the BK models from various sinusoidal profiles from Table 1 are shown in Figure 3. As shown in Table 1, a wide range of variations in ROC and SA (maximum SA between 2° and 72° and minimum ROC between 1 µm and 507 µm) were considered for comparison. Sinusoidal profiles are simulated by defining the height and pitch values as the input parameters. Enlarging the height of a sinusoidal profile with a certain pitch results in higher SA and lower ROC values. On the other hand, increasing the pitch value for a fixed height results in lower SA and higher ROC within a profile. To meet the comparison criteria for the BK model, the length of the profile was equal to ten times the pitch value for each case. The general trend in Figure 3 shows that increasing the height and decreasing the pitch values causes the RMS of the differences of the NSFs to increase. There is an insignificant increase in the RMS value (less than 0.02) when the pitch value increases. This increase occurs for the profiles with lower height values.

Table 1. Specifications of the sinusoidal profiles (in terms of pitch and height values) used to compare the far-field scattering fields obtained by the rigorous BEM and approximate BK models (via the RMS of the differences of the NSFs). Min ROCs are in micrometres.

Height/µm / **Pitch/µm**	**1**	**5**	**10**	**15**	**20**
20	Min ROC: 20 Max SA : 9°	Min ROC: 4 Max SA: 38°	Min ROC: 2 Max SA: 57°	Min ROC: 1 Max SA: 67°	Min ROC: 1 Max SA: 72°
30	Min ROC: 45 Max SA: 6°	Min ROC: 9 Max. SA: 27°	Min ROC: 4 Max SA: 46°	Min ROC: 3 Max SA: 57°	Min ROC: 2 Max SA: 64°
40	Min ROC: 81 Max SA: 4°	Min ROC: 16 Max SA: 21°	Min ROC: 8 Max SA: 38°	Min ROC: 5 Max SA: 50°	Min ROC: 4 Max SA: 57°
50	Min ROC: 157 Max SA: 4°	Min ROC: 25 Max SA: 17°	Min ROC: 13 Max SA: 32°	Min ROC: 8 Max SA: 43°	Min ROC: 6 Max SA: 51°
60	Min ROC: 182 Max SA: 3°	Min ROC: 36 Max SA: 15°	Min. ROC: 18 Max SA: 28°	Min ROC: 12 Max SA: 38°	Min ROC: 9 Max SA: 46°
70	Min ROC: 248 Max SA: 2°	Min ROC: 50 Max SA: 13°	Min ROC: 25 Max SA: 24°	Min ROC: 17 Max SA: 34°	Min ROC: 12 Max SA: 42°
80	Min ROC: 324 Max SA: 2°	Min ROC: 65 Max SA: 11°	Min ROC: 32 Max SA: 21°	Min ROC: 22 Max SA: 30°	Min ROC: 6 Max SA: 38°
90	Min ROC: 410 Max SA: 2°	Min ROC: 82 Max SA: 10°	Min ROC: 41 Max SA: 19°	Min ROC: 27 Max SA: 28°	Min ROC: 20 Max SA: 35°
100	Min ROC: 507 Max SA: 2°	Min ROC: 101 Max SA: 9°	Min ROC: 51 Max SA: 17°	Min ROC: 34 Max SA: 25°	Min ROC: 25 Max SA: 32°

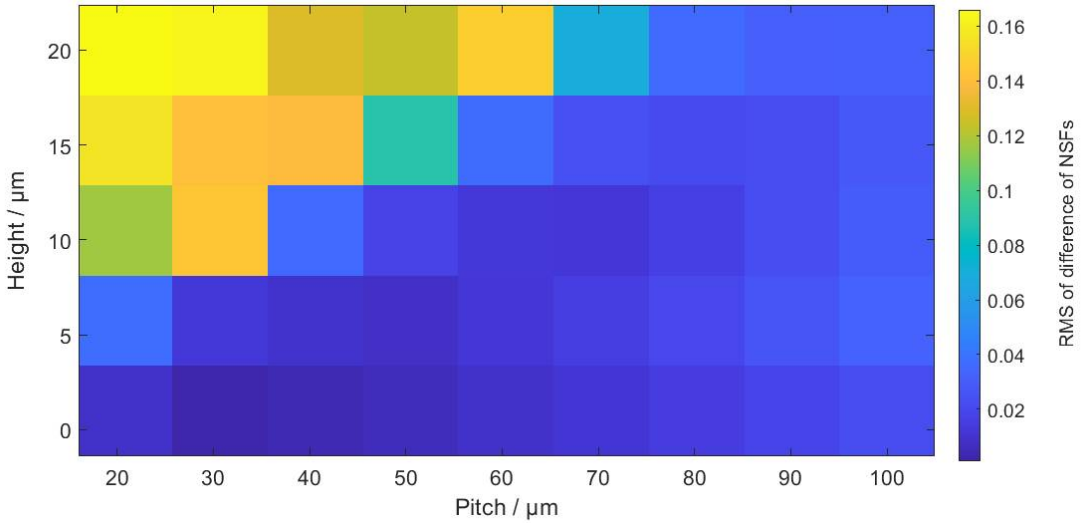

Figure 3. Variations of the RMS of the differences of the NSFs obtained by the BEM and the BK models for the sinusoidal profiles of Table 1 versus changes in the pitch and height values of the profiles. The length of the profiles was considered ten times the pitch value for each case.

1.4 4.2 Comparison of the BEM and the BK models for a range of sinusoidal profiles with a fixed length of 600-µm

If the length of a profile changes, the angular resolution of the calculated far-field scattering varies. To compare the BK and the BEM scattering fields for a set of sinusoidal profiles with a fixed angular resolution, the profiles shown in Table 2 were analysed.

Figure 4 illustrates the variations of the RMS of the differences of the NSFs obtained by the BEM and the BK models for the sinusoidal profiles from Table 2 against changes in the pitch and height values of the profiles. The length of the profiles was 600 µm, so each profile includes at least ten cycles. The far-field scattering was sampled over 2069 observation angles from -88° to 88°. The results are in agreement with those obtained in Figure 2.

Table 2. Specification of the sinusoidal profiles (in terms of pitch and height values) used to compare the far-field scattering fields obtained by the rigorous BEM and approximate BK models (via the RMS of the differences of the NSFs). Min ROCs are in micrometres.

Height/µm / **Pitch/µm**	**2**	**4**	**6**	**8**	**10**
20	Min ROC: 10 Max SA: 17°	Min ROC: 5 Max SA: 32°	Min ROC: 3 Max SA: 43°	Min ROC: 2 Max SA: 51°	Min ROC: 2 Max SA: 57°
30	Min ROC: 23 Max SA: 12°	Min ROC: 11 Max SA: 23°	Min ROC: 8 Max SA: 32°	Min ROC: 6 Max SA: 40°	Min ROC: 4 Max SA: 46°
40	Min ROC: 40 Max SA: 9°	Min ROC: 20 Max SA: 17°	Min ROC: 13 Max SA: 25°	Min ROC: 10 Max SA: 32°	Min ROC: 8 Max SA: 38°
50	Min ROC: 63 Max SA: 7°	Min ROC: 32 Max SA: 14°	Min ROC: 21 Max SA: 21°	Min ROC: 16 Max SA: 27°	Min ROC: 13 Max SA: 32°
60	Min ROC: 91	Min ROC: 46	Min ROC: 30	Min ROC: 23	Min ROC: 18

	Max SA: 6°	Max SA: 12°	Max SA: 17°	Max SA: 23°	Max SA: 28°

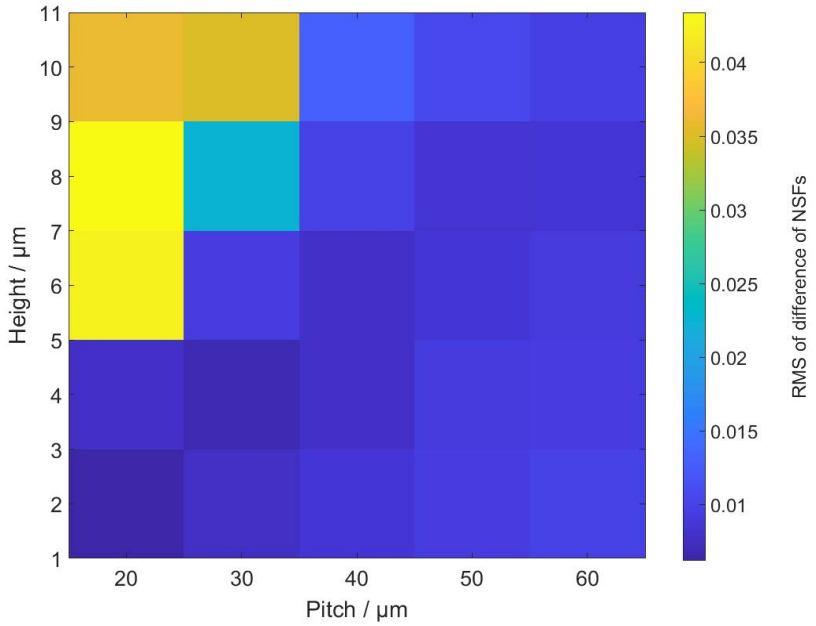

Figure 4. Variations of the RMS of the differences of the NSFs obtained by the BEM and the BK models for the sinusoidal profiles of Table 2 versus changes in the pitch and height values of the profiles. The length of the profiles was 600 µm (including at least ten cycles for each case).

1.5 4.3 Comparison of the BEM and the BK models for a range of sinusoidal profiles with lengths of ten times the pitch values

Figure 5 shows the variations of the RMS of the differences of the NSFs obtained by the BEM and the BK models for the sinusoidal profiles shown in Table 3 against changes in the minimum ROC and maximum SA within the profile. The length of the profiles was considered to be ten times the pitch value for each case. As shown in Figure 5, increasing the maximum SA and decreasing the minimum ROC of the profile causes the RMS of the differences of the NSFs to increase. For the profile with a 5 µm minimum ROC (>> λ), increasing the maximum SA moderately changes the RMS of difference up to 58°. For a profile with a 0.5 µm minimum ROC (≈ λ) increasing the maximum SA (≳ 38°) results in a significant change in the RMS of the difference, indicating that there is a considerable difference between the BK and the BEM scattered fields.

In general, for the approximate BK model to predict the scattered field accurately, it is required that the minimum ROC of the profile is significantly greater than the incident wavelength (≳ 10 λ). Furthermore, even for profiles with a large minimum ROC (5 µm), the BK model is in good agreement with the BEM model if the maximum slope angle of the profile does not exceed a certain value (≲ 38°). For SAs approximately higher than 38°, the BK model fails due to the effects of multiple scattering.

Table 3. Specifications of the sinusoidal profiles (in terms of minimum ROC and maximum SA values) used to compare the scattering far-fields obtained by the rigorous BEM and approximate BK models (via the RMS of the differences of the NSFs). Pitches and heights are in micrometres.

Min ROC /µm / **Max SA /deg**	**0.5**	**2.5**	**5**

18	Pitch: 1 Height: 0.10	Pitch: 5 Height: 0.50	Pitch: 10 Height: 1
28	Pitch: 1.6 Height: 0.27	Pitch: 8.1 Height: 1.35	Pitch: 16.2 Height: 2.70
38	Pitch: 2.6 Height: 0.65	Pitch: 12 Height: 3	Pitch: 24 Height: 6
58	Pitch: 5.1 Height: 2.55	Pitch: 25 Height: 12.50	Pitch: 50 Height: 25
72	Pitch: 10 Height: 10	Pitch: 50 Height: 50	-

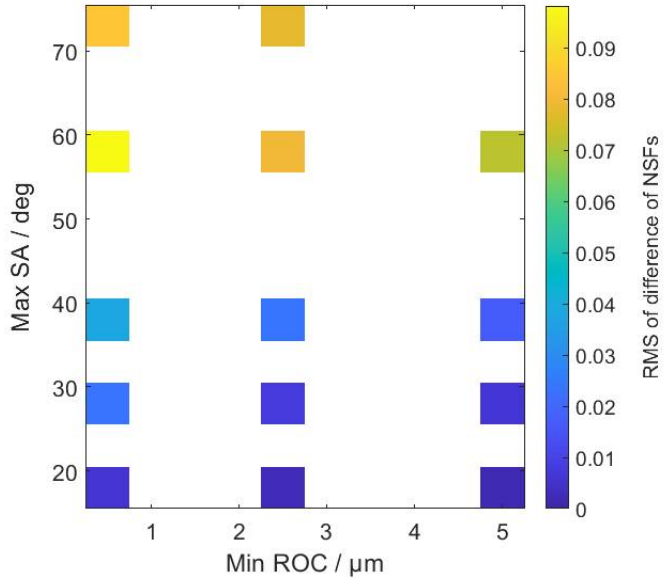

Figure 5. Variations of the RMS of the difference of the NSFs obtained by the BEM and the BK models regarding the sinusoidal profiles of Table 3 versus changes of the minimum ROC and maximum SA values of the profile. The length of the profiles was considered 10 times the pitch value for each case.

5. CONCLUSIONS

In this paper, the validity conditions of the approximate BK model were investigated by comparing the far-field scattering data obtained by the BK model and a rigorous BEM model. The comparison of the BK and the BEM models was quantified by the RMS of the differences of the normalised far-field scattering data. The scattered fields from a range of various sinusoidal profiles with different ROCs and SAs (using a range of different pitch and height values) were simulated using the approximate BK model and the rigorous BEM model. Variations of the RMS of the differences of the normalised scattered fields were investigated in terms of the change in the minimum ROC and maximum SA of the profiles. In order to satisfy the main validity condition of the BK model, the minimum ROC of the profile should be significantly large compared to the wavelength of the incident light (approximately ten times or larger). It is also shown that the presence of SAs approximately higher than 38° within a profile causes the effect of multiple scattering to appear, which in turn results in the failure of the BK model.

In future work, we plan to compare the angular distribution of the scattered fields from a combination of sinusoidal profiles obtained by the BEM and the BK models. The combination of sinusoidal profiles with different pitch and height values results in generating profiles within a wide range of radii of curvature and slope angles, which enable us to define more accurate conditions in which the approximate BK model is valid.

6. ACKNOWLEDGEMENTS

The authors would like to thank Dr Nikolay Nikolaev (Loughborough University) and Dr Rong Su (Shanghai Institute of Optics and Fine Mechanics) for the use of the BEM and BK codes, respectively, and also UKRI Research England Development (RED) Fund for supporting this work via the Midlands Centre for Data-Driven Metrology. This work was supported by the European Metrology Programme for Innovation and Research (EMPIR) project [TracOptic, 20IND07] and the European Union's Horizon 2020 Research and Innovation programme [DAT4.ZERO, 958363].

REFERENCES

[1] Sheppard, C. J. R., "Scattering and the Spatial Frequency Representation," in [Light Scattering and Nanoscale Surface Roughness], Maradudin, A. A., Ed., Springer US, Boston, MA, 61-92 (2007).
[2] Beckmann, P. and Spizzichino, A., [The Scattering of Electromagnetic Waves from Rough Surfaces], Artech House, Norwood, MA, (1987).
[3] Larkin, K. G., "Efficient nonlinear algorithm for envelope detection in white light interferometry," J. Opt. Soc. Am. A 13(4), 832-843 (1996).
[4] de Groot, P. and Deck, L., "Surface Profiling by Analysis of White-light Interferograms in the Spatial Frequency Domain," J. Mod. Opt. 42(2), 389-401 (1995).
[5] Kiselev, I., Kiselev, E. I., Drexel, M. and Hauptmannl, M., "Noise robustness of interferometric surface topography evaluation methods. Correlogram correlation," Surf. Topogr.: Metrol. Prop. 5(4), 045008 (2017).
[6] Helmli, F., "Focus Variation Instruments," in [Optical Measurement of Surface Topography], Leach, R K., Ed., Springer Berlin, Heidelberg, 131-166 (2011).
[7] Artigas, R., "Imaging Confocal Microscopy," in [Optical Measurement of Surface Topography], Leach, R. K., Ed., Springer Berlin, Heidelberg, 237-286 (2011).
[8] Taflove, A. and Hagness, S. C., [Computational Electrodynamics: The Finite-difference Time-domain Method], Artech House, Boston, (2005).
[9] Elschner, J., Hinder, R. and Schmidt, G., "Finite Element Solution of Conical Diffraction Problems," Adv. Comput. Math 16(2), 139-156 (2002).
[10] Moharam, M. G. and Gaylord, T. K., "Rigorous coupled-wave analysis of grating diffraction— E-mode polarization and losses," J. Opt. Soc. Am. 73(4), 451-455 (1983).
[11] Harrington, R. F., [Field Computation by Moment Methods], John Wiley & Sons, Inc., New York, (1993).
[12] Pahl, T., Hagemeier, S., Bischoff, J., Manske, E. and Lehmann, P., "Rigorous 3D modeling of confocal microscopy on 2D surface topographies," Meas. Sci. Technol. 32(9), 094010 (2021).
[13] Pahl, T., Hagemeier, S., Künne, M., Yang, D. and Lehmann, P., "3D modeling of coherence scanning interferometry on 2D surfaces using FEM," Opt. Express 28(26), 39807-39826 (2020).
[14] de Groot, P., de Lega, X. C., Liesener, J. and Darwin, M., "Metrology of optically-unresolved features using interferometric surface profiling and RCWA modeling," Opt. Express 16(6), 3970-3975 (2008).
[15] Pahl, T., Hagemeier, S., Hüser, L., Xie, W. and Lehmann, P., "Two-dimensional modelling of systematic surface height deviations in optical interference microscopy based on rigorous near field calculation," J. Mod. Opt. 67(11), 963-973 (2020).
[16] Fu, L., Frenner, K. and Osten, W., "Rigorous Speckle Simulation Using Surface Integral Equations and Boundary Element Methods," [Fringe 2013: 7th International Workshop on Advanced Optical Imaging and Metrology], Springer-Verlag, Berlin, Heidelberg, 361-364 (2014).
[17] Salinas, F. S., Lancaster, J. L. and Fox, P. T., "3D modeling of the total electric field induced by transcranial magnetic stimulation using the boundary element method," Phys. Med. Biol. 54(12), 3631-3647 (2009).
[18] Bai, M. R., "Application of BEM (boundary element method)-based acoustic holography to radiation analysis of sound sources with arbitrarily shaped geometries," J. Acoust. Soc. Am. 92(1), 533-549 (1992).
[19] Manara, G., Monorchio, A. and Rosace, S., "A stable time domain boundary element method for the analysis of electromagnetic scattering and radiation problems," Eng. Anal. Bound. Elem. 27(4), 389-401 (2003).
[20] Thomas, M., Su, R., Nikolaev, N., Coupland, J. and Leach, R. K., "Modeling of interference microscopy beyond the linear regime," Opt. Eng. 59(3), 034110 (2020).
[21] Thomas, M., Su, R., de Groot, P., Coupland, J. and Leach, R. K., "Surface measuring coherence scanning interferometry beyond the specular reflection limit," Opt. Express 29(22), 36121-36131 (2021).

[22] Liu, M., Fai Cheung, C., Senin, N., Wang, S., Su, R. and Leach, R., "On-machine surface defect detection using light scattering and deep learning," J. Opt. Soc. Am. A 37(9), B53-B59 (2020).
[23] Sheppard, C. J. R., "Imaging of random surfaces and inverse scattering in the Kirchoff approximation," Waves in Random Media 8(1), 53-66 (1998).
[24] Born, M. and Wolf, E., [Principles of Optics: Electromagnetic Theory of Propagation, Interference and Diffraction of Light], Cambridge University Press, Cambridge, (1999).
[25] de Groot, P. J. and Colonna de Lega, X., "Fourier optics modeling of interference microscopes," J. Opt. Soc. Am. A 37(9), B1-B10 (2020).
[26] Rice, S. O., "Reflection of electromagnetic waves from slightly rough surfaces," Commun. Pure Appl. Math. 4(2-3), 351-378 (1951).
[27] Coupland, J., Mandal, R., Palodhi, K. and Leach, R. K., "Coherence scanning interferometry: linear theory of surface measurement," Appl. Opt. 52(16), 3662-3670 (2013).
[28] Xie, W., Lehmann, P., Niehues, J. and Tereschenko, S., "Signal modeling in low coherence interference microscopy on example of rectangular grating," Opt. Express 24(13), 14283-14300 (2016).
[29] Mandal, R., Coupland, J., Leach, R. K. and Mansfield, D., "Coherence scanning interferometry: measurement and correction of three-dimensional transfer and point-spread characteristics," Appl. Opt. 53(8), 1554-1563 (2014).
[30] Nikolaev, N., Petzing, J. and Coupland, J., "Focus variation microscope: linear theory and surface tilt sensitivity," Appl. Opt. 55(13), 3555-3565 (2016).
[31] Harvey, J., Krywonos, A. and Vernold, C., "Modified Beckmann-Kirchhoff scattering model for rough surfaces with large incident and scattering angles," Opt. Eng. 46(7), 078002 (2007).
[32] Schröder, S., Duparré, A., Coriand, L., Tünnermann, A., Penalver, D. H. and Harvey, J. E., "Modeling of light scattering in different regimes of surface roughness," Opt. Express 19(10), 9820-9835 (2011).
[33] Liu, M., Senin, N., Su, R. and Leach, R. K., "Measurement of laser powder bed fusion surfaces with light scattering and unsupervised machine learning," Meas. Sci. Technol. 33(7), 074006 (2022).
[34] Thorsos, E. I. and Jackson, D. R., "Studies of scattering theory using numerical methods," Waves in Random Media 1(3), S165-S190 (1991).
[35] McCammon, D. F. and McDaniel, S. T., "Surface reflection: On the convergence of a series solution to a modified Helmholtz integral equation and the validity of the Kirchhoff approximation," J. Acoust. Soc. Am. 79(1), 64-70 (1986).
[36] Chen, J. S. and Ishimaru, A., "Numerical simulation of the second-order Kirchhoff approximation from very rough surfaces and a study of backscattering enhancement," J. Acoust. Soc. Am. 88(4), 1846-1850 (1990).
[37] Simonsen, I., "Optics of surface disordered systems," Eur. Phys. J. Spec. Top. 181(1), 1-103 (2010).
[38] Maradudin, A. A., Michel, T., McGurn, A. R. and Méndez, E. R., "Enhanced backscattering of light from a random grating," Ann. Phys. (N. Y.) 203(2), 255-307 (1990).
[39] Sein, J. J., "A note on the Ewald-Oseen extinction theorem," Opt. Commun. 2(4), 170-172 (1970).
[40] Su, R., Coupland, J., Sheppard, C. and Leach, R. K., "Scattering and three-dimensional imaging in surface topography measuring interference microscopy," J. Opt. Soc. Am. A 38(2), A27-A42 (2021).